Iron nanoparticles for plant nutrition: Synthesis, transformation, and utilization by the roots of *Cucumis sativus*

Maria Gracheva[1,2], Zoltán Klencsár[2], Viktória Kovács Kis[2,3], Kende Attila Béres[1,4],
Zoltán May[4], Viktória Halasy[5], Amarjeet Singh[6], Ferenc Fodor[6], Ádám Solti[6],
László Ferenc Kiss[7], Gyula Tolnai[8], Zoltán Homonnay[1], Krisztina Kovács[1,a]

[1] Laboratory of Nuclear Chemistry, Institute of Chemistry, ELTE Eötvös Loránd University, Pázmány Péter sétány 1/A, Budapest 1117, Hungary
[2] Centre for Energy Research, Konkoly-Thege Miklós út. 29-33, Budapest 1121, Hungary
[3] Department of Mineralogy, ELTE Eötvös Loránd University, Pázmány Péter sétány 1/C, Budapest 1117, Hungary
[4] Institute of Materials and Environmental Chemistry, Research Centre for Natural Sciences, Magyar tudósok körútja 2, Budapest 1117, Hungary
[5] Department of Anatomy, Histology and Embryology, Faculty of Medicine, Semmelweis University, Budapest 1094, Hungary
[6] Department of Plant Physiology and Molecular Plant Biology, Institute of Biology, ELTE Eötvös Loránd University, Pázmány Péter sétány 1/C, Budapest 1117, Hungary
[7] Wigner Research Centre for Physics, Konkoly-Thege Miklós út. 29-33, Budapest 1121, Hungary
[8] Budapest, Hungary
a) Address all correspondence to this author. e-mail: krisztina.kovacs@ttk.elte.hu
Zoltán Homonnay was a guest editor of this journal during the review and decision stage. For the JMR policy on review and publication of manuscripts authored by editors, please refer to http://www.mrs.org/editor-manuscripts/.

Nanotechnology has been evolving in the past decades as an alternative to conventional fertilizers. Ferrihydrite nanoparticles that model the available Fe pool of soils are proposed to be used to recover Fe deficiency of plants. Nevertheless, ferrihydrite aqueous suspensions are known to undergo slow transformation to a mixture of goethite and hematite, which may influence its biological availability. Several nanocolloid suspensions differing in the surfactant type were prepared for plant treatment and fully characterized by transmission electron microscopy and ^{57}Fe Mössbauer spectroscopy supported by magnetic measurements. The rate of transformation and the final mineral composition were revealed for all the applied surfactants. Nanomaterials at different stages of transformations were the subject of plant physiological experiments aiming at comparing the behavior and plant accessibility of the manufactured suspensions of nanoscale iron(III) oxide and oxide–hydroxide particles.

Introduction

The production and industrial application of nanomaterials increase rapidly every year drawing more and more attention to the possible effects associated with the release of nanoparticles to the environment [1–3]. Nanoparticles, being one of the basic building blocks of nanotechnology, can be found nowadays to play a role in various fields from magnetic devices to sunscreen products [4, 5]. It is inevitable that a considerable fraction of the produced nanoparticles will finally find its way to different environmental compartments such as air, water, and soil [6]. Despite growing concerns regarding the potential harmful

effects and biological toxicity, little is known about their transport, possible transformations, and final fate in the ecosystems [7]. Although release of nanoparticles to the environment can be usually expected to be unfavorable to living beings, in some cases, deliberate exposure of plants to specific nanoparticles may be beneficial especially in the micronutrient homeostasis.

Iron is known to be an essential micronutrient for plants because it plays a vital role in cells construction and metabolic processes such as DNA synthesis, respiration, and photosynthesis. Therefore, disturbed iron uptake is one of the limiting factors of plant biomass production. Nanoparticle-based iron

fertilizers are suggested to have a great potential in agriculture because of their low cost and low toxicity [8] and can serve as a biologically available Fe pool for plants retained in soil. Recent studies have used various Fe nanoparticles to investigate their beneficial effect on plant growth and metabolism [9, 10]. Ferrihydrite, a poorly crystalline form of iron-oxyhydroxide with a variable stoichiometry depending on its level of hydration, occurs in many soils in the form of nanoparticles attached to the surface of other soil components like clay minerals [11, 12]. For agricultural applications, ferrihydrite is believed to be one of the most promising candidates among nanoscale Fe-oxides/hydroxides because of its relatively high solubility [13].

Ferrihydrite aqueous suspensions are known to undergo slow transformation to goethite, hematite, lepidocrocite, magnetite, and green rusts or mixture of these compounds depending on the experimental conditions such as temperature, pH, particle size, and the presence of other ions and ligands [14–16]. Such transformations play an essential role in Fe mineralogy in various natural environments, including soils. Both hematite and goethite are thermodynamically more stable than ferrihydrite and their formation occurs through competing mechanisms, while hematite is crystallized via dehydration and internal atomic rearrangements within particles aggregation, goethite is formed from dissolved Fe^{3+} via the formation of Fe–OH–Fe and Fe–O–Fe bridges and condensation. These structural changes can also affect the biological availability of Fe, thus they could significantly influence the effectiveness of these nano-Fe-oxides as iron fertilizers in soils.

The present work describes a long-term experiment on studying properties, transformation, and plant accessibility of synthetically prepared suspensions of nano-Fe-oxide particles. Several nanocolloid suspensions of ferrihydrite differing in the applied surfactant [S0 (Priowax 200), S1(PEG-1500), S2(Emulsion 104D), S3(SOLUTOL HS 15), see Methods and Materials section for the details] were prepared and fully characterized by transmission electron microscopy, ^{57}Fe Mössbauer spectroscopy, and magnetization measurements before the plant treatment. To investigate the time dependent aging of the nanomaterials, spectra were recorded after various time periods after the preparation. The effect of surfactants on the transformation rate and final mineral composition was revealed.

The utilization of Fe from the nanoparticles was subsequently studied by applying the suspension as the source of Fe for cucumber (*Cucumis sativus*) model. Cucumber operates an effective, reduction-based Fe uptake mechanism (also known as Strategy I) but sensitive enough for Fe deficiency that makes it an appropriate model to address plant nutrition and agricultural experiments [17]. Iron deficiency triggers Fe deficiency responses in Strategy I plants such as upregulated expression of *Ferric Reductase Oxidase* (*FRO*) genes and enhanced root ferric chelate reductase (FCR) activity [18]. In turn, Fe resupply

leads to the suppression of these deficiency responses, which protect the roots against Fe overaccumulation. In the suppression of iron deficiency responses, hemerythrin domain Fe sensors of the plant cells have crucial role, their activation results in the elimination of the FRO transcripts [19]. The turnover of FRO proteins in the plasma membrane finally restore the original FCR activity of the roots [20]. Since the restoration of iron deficiency responses are highly dependent on Fe sensing mechanisms, decrease in both the FRO transcript amount and in the FCR activity indicate the availability of Fe for the model plant. Therefore, to test the agronomical potential in the beneficial effect of Fe nanoparticles, the recovery of iron deficiency in plants was followed by measurements of the enzymatic activity of the FCR enzyme and by the upregulated expression of FRO genes.

Results

Transformation of the materials S0 and S0(^{57}Fe)

The nanocolloid suspension S0 was already successfully applied in plant nutrition, the corresponding results are summarized in Singh et al. [21]. TEM images taken on the as-prepared sample accompanied with X-ray diffraction studies performed on an analogous dried nanoparticle powder [22] showed the presence of only ferrihydrite particles. However, later analysis revealed a slow transformation of the material despite the presence of surfactant. TEM results on the same sample measured 1500 days later showed that significant part of the sample was transformed to nanohematite (Fig. 1). The pH was found to slightly decrease with time (Suppl. Table 1). The ^{57}Fe Mössbauer spectrum of the frozen suspension measured 150 days after preparation exhibited the relative spectral area fraction of 20(4)% associated with magnetic component [22] that can be identified as hematite based on the subsequent TEM results. With respect to the 5 nm diameter of the ferrihydrite nanoparticles in the as-prepared suspension, the larger size (up to ~20 nm) of the detected hematite nanoparticles corroborates that the formation of hematite proceeds via an aggregation step of ferrihydrite nanoparticles.

In order to clarify the transformation process, the sample S0(^{57}Fe) enriched with ^{57}Fe was prepared with the same surfactant as S0. The pH of the S0(^{57}Fe) nanocolloid suspension did not change significantly during the period of investigation (Suppl. Table 1). According to the TEM images taken shortly after its preparation [Fig. 2(a)], the suspension S0(^{57}Fe) includes nanoparticles (diameter of 2–7 nm) with typically low crystallinity. Their lattice parameters correspond to ferrihydrite structure. Larger, typically round-shaped particles with various sizes below 10 nm [Fig. 2(a–c)] appear to be formed via aggregation and may represent an intermediate stage towards the formation of well-crystallized particles of goethite or hematite.
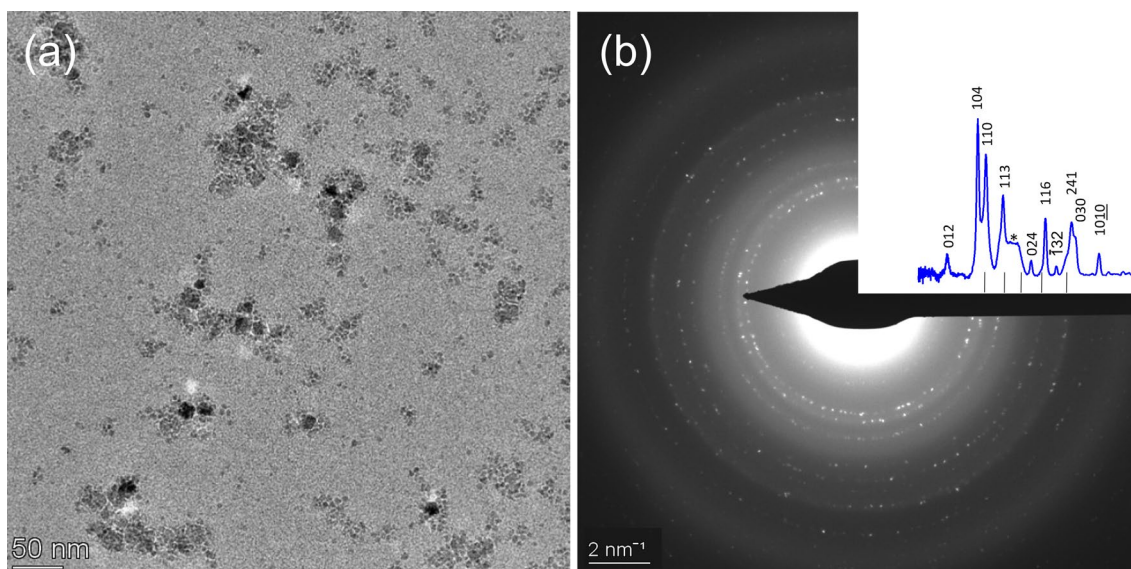
Figure 1: (a) Bright-field image and (b) SAED pattern of the S0 colloid suspension 1500 days after preparation. Indices of hematite are given on the background subtracted integrated intensity profile. Sticks below the intensity profile indicate diffraction peaks of 6-line ferrihydrite [23]. Elevated background indicated by asterisk is from amorphous carbon (residue of surfactant).
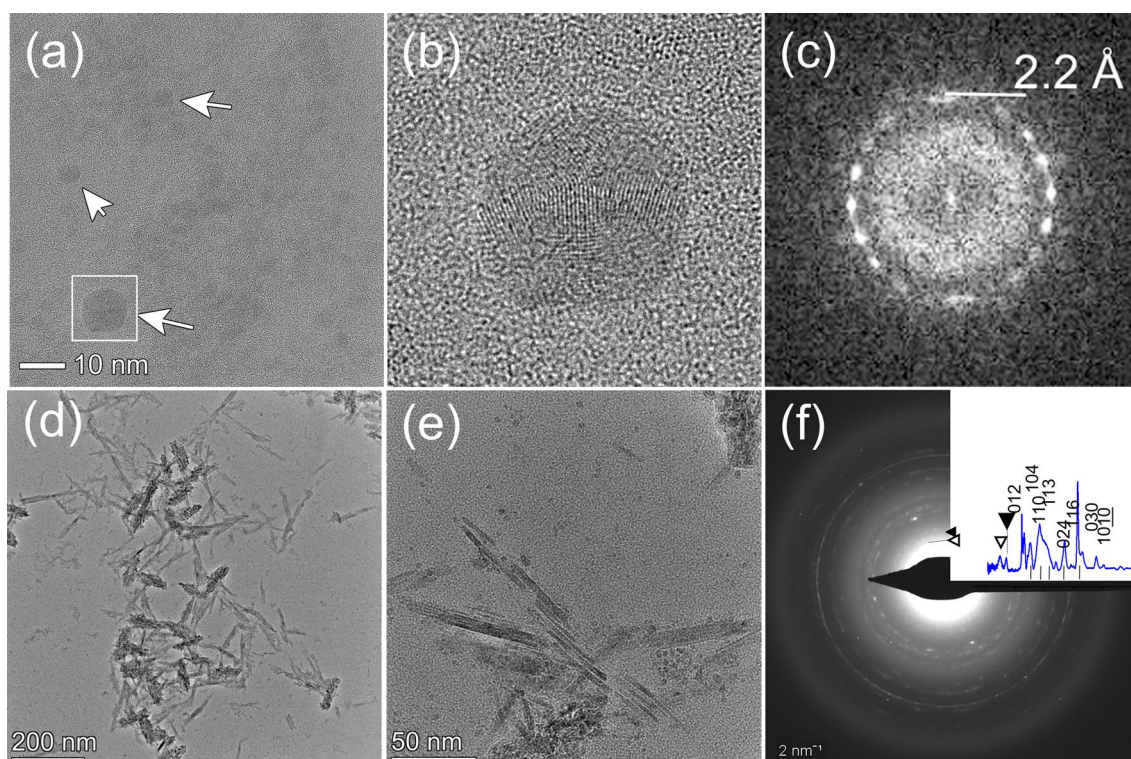

Figure 2: Characteristics of the S0(^{57}Fe) colloid suspension shortly after its preparation (a–c) and 1000 days after preparation (d–f): (a) bright-field image of typical isometric particles with various sizes around and below 10 nm, with arrows indicating larger, round-shaped particles, (b) high-resolution image of the particle framed on the left image and (c) its Fourier transform showing polycrystalline structure and increased crystallinity with respect to that of the smallest particles, which implies the formation via aggregation of individual smaller domains, (d) bright-field image of typical needle-shape particles, (e) high-resolution image of the particles from the image (d), (f) SAED pattern of the S0(^{57}Fe) colloid suspension 1000 days after preparation. Diagnostic reflections for goethite and hematite at 4.2 Å and 3.7 Å are indicated by white and black arrowheads, respectively. Further intense peaks of hematite are indexed on the background subtracted integrated intensity profile. Sticks below the intensity profile indicate diffraction peaks of 6-line ferrihydrite [23].

To investigate the aging process of the material in details, several Mössbauer spectra were measured after different time periods: 10, 250, 500, 800, and 1000 days after the suspension preparation (Fig. 3, spectrum of the sample after 250 days after preparation is shown in [21]). Mössbauer spectrum of the frozen S0(^{57}Fe) colloid suspension recorded on the 10th day after preparation (Fig. 3) can be fitted with a model consisting of a quadrupole doublet, two magnetic sextets, and a broad component referring to magnetic relaxation effects (Suppl. Table 2). The doublet is characterized with an ^{57}Fe isomer shift of $\delta = 0.45(1)$ mm/s and a quadrupole splitting of $\Delta = 0.69(1)$ mm/s. These parameters are indicative of the high-spin Fe(III) state. By taking into account also the TEM results [Fig. 2(a)], the doublet component may be associated with ferrihydrite nanoparticles. The doublet component accounts for 69% of the total spectral area, indicating that in the S0(^{57}Fe) colloid suspension ca. 69% of iron is situated in ferrihydrite nanoparticles, the latter representing the majority of the colloids at this moment of time.

Isomer shifts of the sextets ($\delta_1 = 0.49 \pm 0.01$ mm/s, $\delta_2 = 0.48 \pm 0.01$ mm/s) and that of the broad component ($\delta_r = 0.51 \pm 0.04$ mm/s) suggest the presence of only ferric iron

in the sample at the moment of measurement. The precise identification of these iron phases is hindered by the rather low intensities of the sextets with respect to the statistical noise of the spectrum, and by the fact that different ferric oxyhydroxides and hydrous oxides have close-lying isomer shifts [24]. However, comparison with the TEM images allows to assume that the broad component and the sextets correspond to the hematite and goethite particles on the intermediate and the final stages of formation, respectively.

Mössbauer spectra of the frozen S0(^{57}Fe) colloid suspension recorded later were evaluated simultaneously with a model consisting of two quadrupole doublets, two magnetic sextets, and a broad component associated with magnetic relaxation effects (Suppl. Table 3). As described earlier, the main iron(III) doublet corresponds to ferrihydrite nanoparticles, while the component reflecting magnetic relaxation effects can be associated with the aggregated ferric particles undergoing the transformation from ferrihydrite to hematite/goethite. The magnetic components ($\delta_1 = \delta_2 = 0.47(1)$ mm/s, $2\varepsilon_1 = -0.17(3)$ mm/s, $2\varepsilon_2 = -0.30(4)$ mm/s, $B_{hf1} = 52.0(1)$ T, $B_{hf2} = 48.0(2)$ T) can be associated with larger particles of hematite and goethite, respectively. The
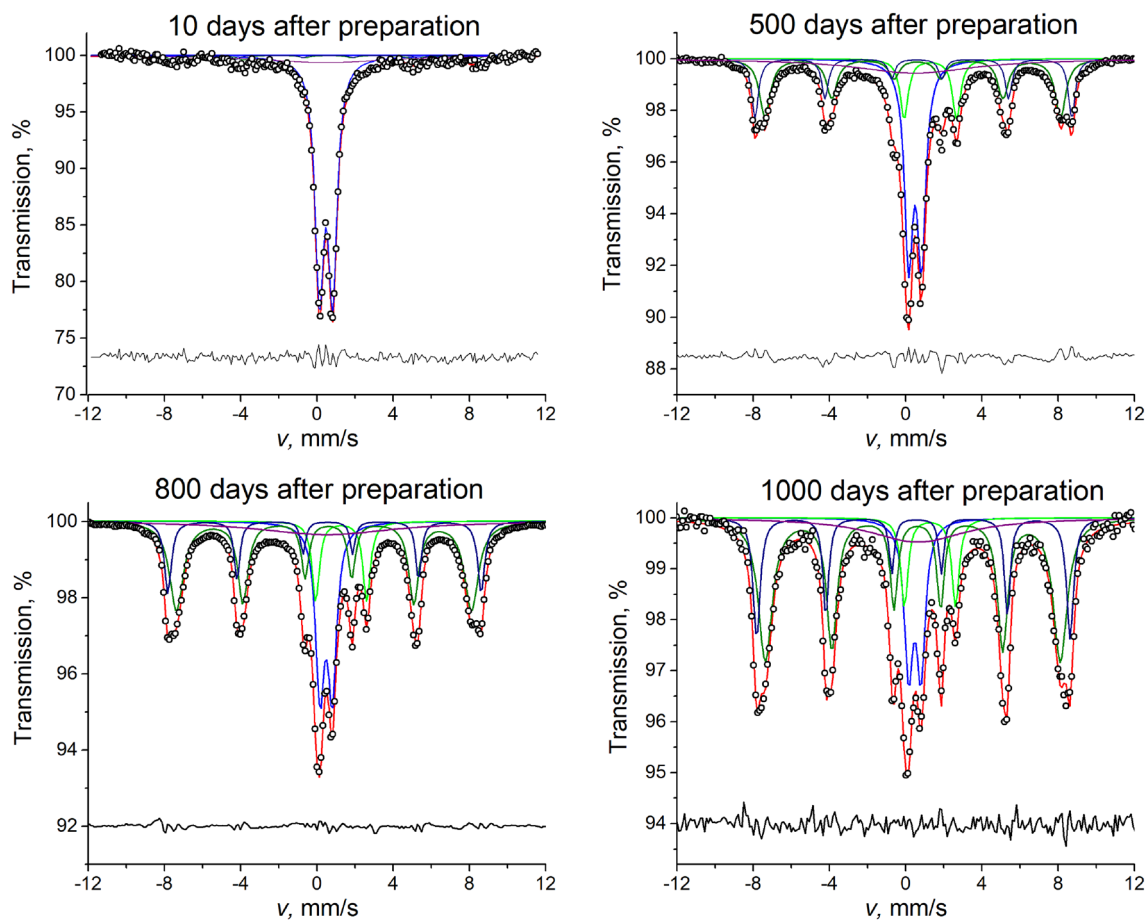

Figure 3: Mössbauer spectra of the frozen S0(^{57}Fe) colloid suspension sample ($T = 80$ K) measured at different time points.

relative content of a newly appeared iron(II) doublet ($\delta = 1.26(1)$ mm/s, $\Delta = 2.68(3)$ mm/s) is 10% after 250 days passed after preparation and it slowly decreases with time (Fig. 4). This component may correspond to iron(II) in a structure of a mixed-valence mineral formed during the transformation.

In contrast to the slow rate of degradation of the iron(II) component, the relative spectral area of the Fe(III) doublet decreases dramatically (from 87 to 15%) during the investigation period, while the relative spectral area of the magnetic components increases with time, showing a slow transformation of ferrihydrite into a mixture of hematite and goethite with the prevalence of the latter.

TEM images taken 1000 days after preparation [Fig. 2(d–f)] also exhibit the presence of goethite and hematite. Goethite crystals are generally needle like in morphology and vary in size. The majority is in the range of 5–10 nm wide and 50–100 nm long.

Comparison of different surfactants

To compare the influence of the surfactant on the rate of the transformation the suspensions S1, S2, and S3 were studied by means of Mössbauer spectroscopy and TEM at two different time points: shortly after preparation and 6 years later. In addition, in order to monitor the possible intermediate formation of dissolved paramagnetic iron species during the transformation process, FC/ZFC magnetization measurements were performed on the samples ca. 20 months after the first TEM measurements. The pH values of the suspensions were close to each other after the preparation, and did not change significantly during the

whole investigation period (Suppl. Table 1). Mössbauer spectra of suspensions were fitted using a model consisted of two quadrupole doublets and a sextet. Obtained Mössbauer parameters are shown in Suppl. Tables 2 and 3.

TEM-SAED images of the S1 suspension shortly after preparation (Fig. 5) showed that the sample consists of homogeneous 6-line ferrihydrite particles with size in the range of 4–7 nm. Mössbauer analysis confirmed this observation exhibiting only one ferric component with parameters typical for Fe nuclei in the structure of ferrihydrite. As in the case of S0(^{57}Fe), the presence of a small amount of iron(II) was detected in the sample. The spectrum of the aged suspension also showed no magnetic components. The only observed change was the disappearance of the iron(II) doublet, referring to the oxidation of the corresponding iron species. TEM investigations exhibited the aggregation of particles that were earlier arranged homogeneously (Fig. 5), though no increase of individual particle size occurred. Broad diffuse rings indicate that ferrihydrite is still present in the suspension as the dominant phase. Sticks below the intensity profile indicate diffraction peaks of 6-line ferrihydrite [23]. Nevertheless, faint spotty reflections along diffraction rings indicated by arrowheads in Fig. 5 definitely prove the appearance of minor amount of hematite.

In contrast to the previous case, Mössbauer spectrum and TEM images of suspension S2 measured shortly after the preparation (Fig. 6) already showed the presence of appreciable amount of hematite. The corresponding Mössbauer spectrum (Fig. 6, left) is consistent with above 20% of iron being incorporated into the structure of hematite nanoparticles. The
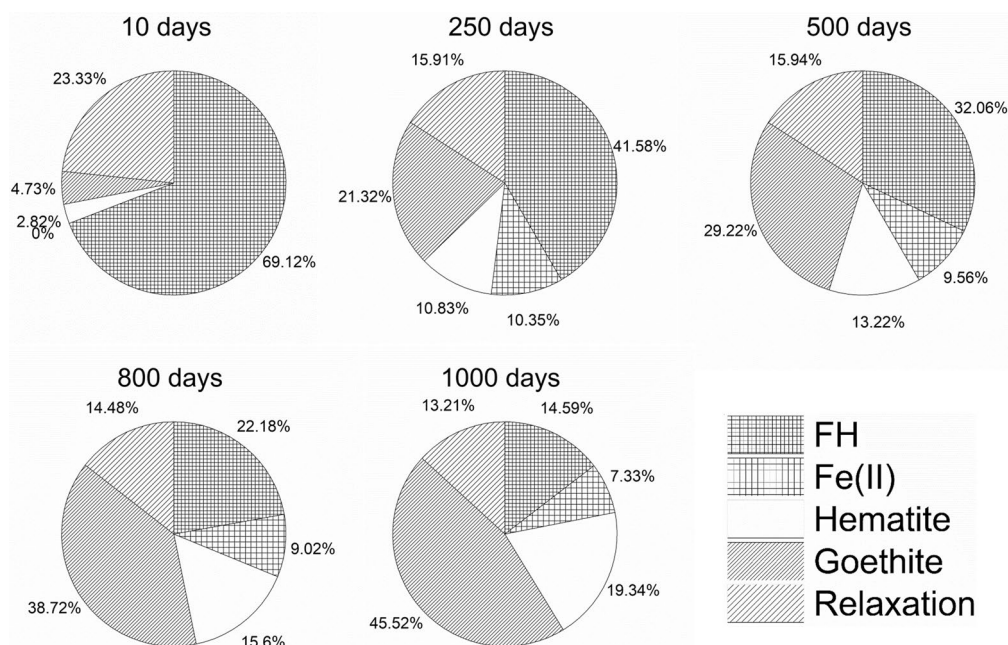

Figure 4: Diagram charts showing the relative areas of spectral components identified in the Mössbauer spectra of S0(^{57}Fe) frozen colloid suspension as being associated with the different phases indicated on the legend.
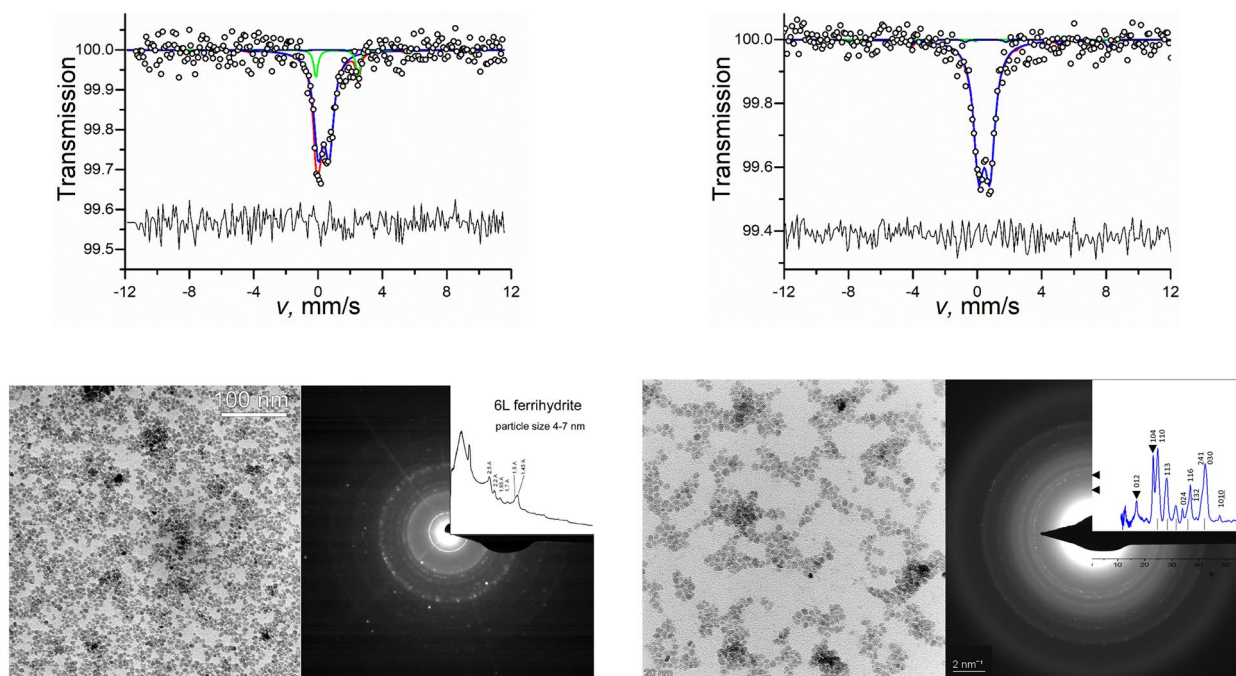
Figure 5: Mössbauer spectra, bright-field images and SAED patterns of S1 suspension shortly after preparation (left) and 6 years later (right). Indices of most intense peaks are given on the background subtracted integrated intensity profile.
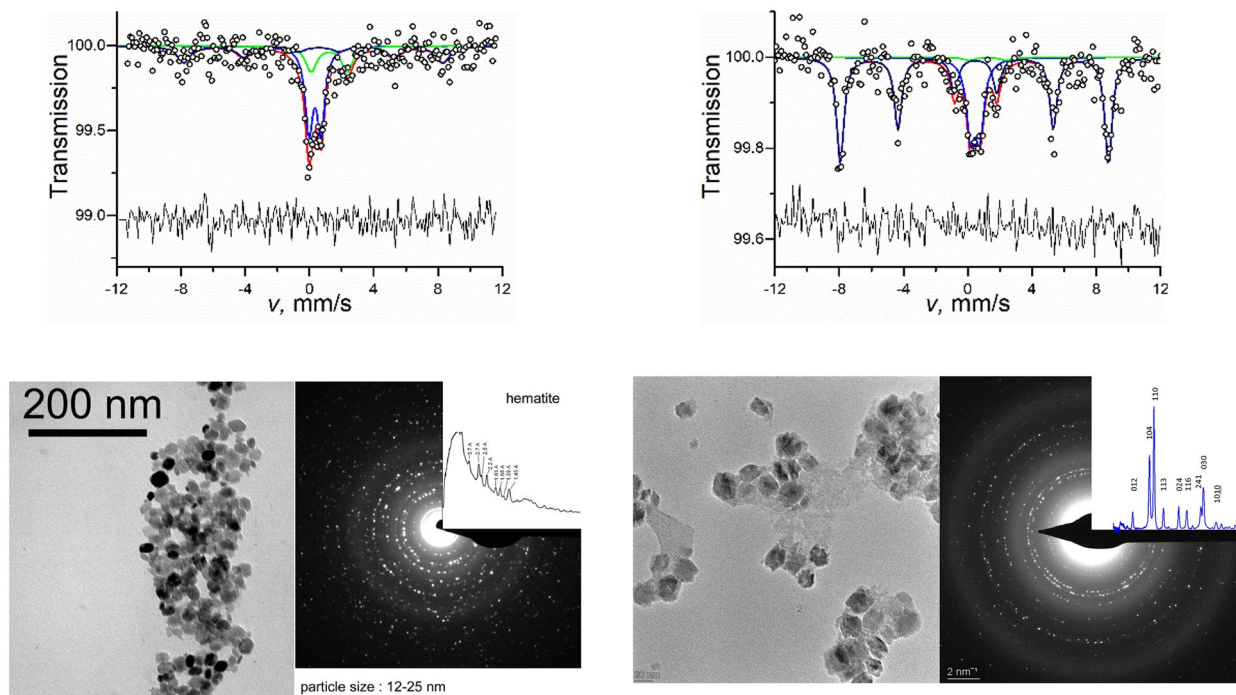

Figure 6: Mössbauer spectra, bright-field images and SAED patterns of S2 suspension shortly after preparation (left) and 6 years later (right). Indices of most intense peaks are given on the background subtracted integrated intensity profile.

particles observed on the bright-field images have a diameter in the range of 12–25 nm and possess irregular hexagonal shape typical for hematite. The presence of a small amount of iron(II)

was found in this sample as well. The investigation of the aged sample clearly showed the progress of the transformation. With the passing of time the relative area of the sextet component

($\delta = 0.45(2)$ mm/s, $2\varepsilon = -0.08(3)$ mm/s, $B_{hf} = 51.9(3)$ T) has increased substantially to 71%. On the TEM micrographs one can observe the agglomerates of hematite particles connected with, presumably, the surfactant substance. SAED indicates the sample to consist of pure nanocrystalline hematite.

Mössbauer spectrum of the suspension S3 shortly after preparation (Fig. 7) was fitted using the same model as in the case of S2, suggesting that beside ferrihydrite, iron(II) and hematite are present in the sample. TEM study proved the suspension to consist mainly of nanoparticles of 6-line ferrihydrite (4–8 nm), mixed with minor amounts of larger particle size hematite. As the time passed, the sample was still found to consist of a mixture of ferrihydrite and hematite. The 104 diffraction peak of hematite is well separated in the aged sample, while it is missing in the as-prepared sample. This observation indicates increasing hematite content during aging but most of the particles were found to be polycrystalline. It is also remarkable that despite the similarity of parameters of Mössbauer spectra of aged samples S2 and S3, the size of hematite particles is much smaller in the case of S3 than in S2 at this stage of aging. Additionally, SAED pattern of the S3 sample after transformation indicates the presence of another minor phase with lattice distance of approximately 3 Å (marked with black arrowhead), which is presumably maghemite. Since the average size of the particles of this phase is below 10 nm, it should appear as a superparamagnetic doublet in the Mössbauer spectrum [13, 24] with parameters very close to the

ones of ferrihydrite, therefore, it cannot be distinguished in the present spectra.

The FC/ZFC measurements of the samples, carried out at an intermediate time point, resulted in the close-lying curves shown in Suppl. Fig. 1. The curve associated with sample S1 is shown in Fig. 8 in comparison with the FC/ZFC curves obtained for the sample S0(^{57}Fe)$_{intermediate}$. The latter reflects mainly a paramagnetic contribution originating from the precursor ^{57}FeCl$_3$ solution, as in the corresponding stage of preparation the formation of nanoparticles was far from complete yet. The latter is also corroborated by the associated ^{57}Fe Mössbauer spectrum, shown in the inset of Fig. 8, whose profile resembles that (see, e.g., Suppl. Fig. 2) of an ^{57}FeCl$_3$ solution at the same temperature.

In comparison with the paramagnetic behavior of S0(^{57}Fe)$_{intermediate}$, the FC/ZFC magnetization curves of samples S1, S2, and S3 display reduced magnetic moments with a cusp representing magnetic blocking appearing in the ZFC curve at around $T_b = 16$ K (for S1 and S2) and $T_b = 22$ K (for S3), above which the samples display superparamagnetic behavior. The T_{irr} irreversibility temperature, where FC and ZFC curves start to deviate from each other on temperature decrease (see Suppl. Fig. 1), is close to the T_b blocking temperature for sample S3, but lies at higher temperatures for the samples S1 ($T_{irr} \approx 36$ K) and S2 ($T_{irr} \approx 26$ K). The reduction in magnetization with respect to paramagnetic behavior as well as the appearance of magnetic blocking and irreversibility at lower temperatures are consistent with the majority of Fe^{3+} ions being included either
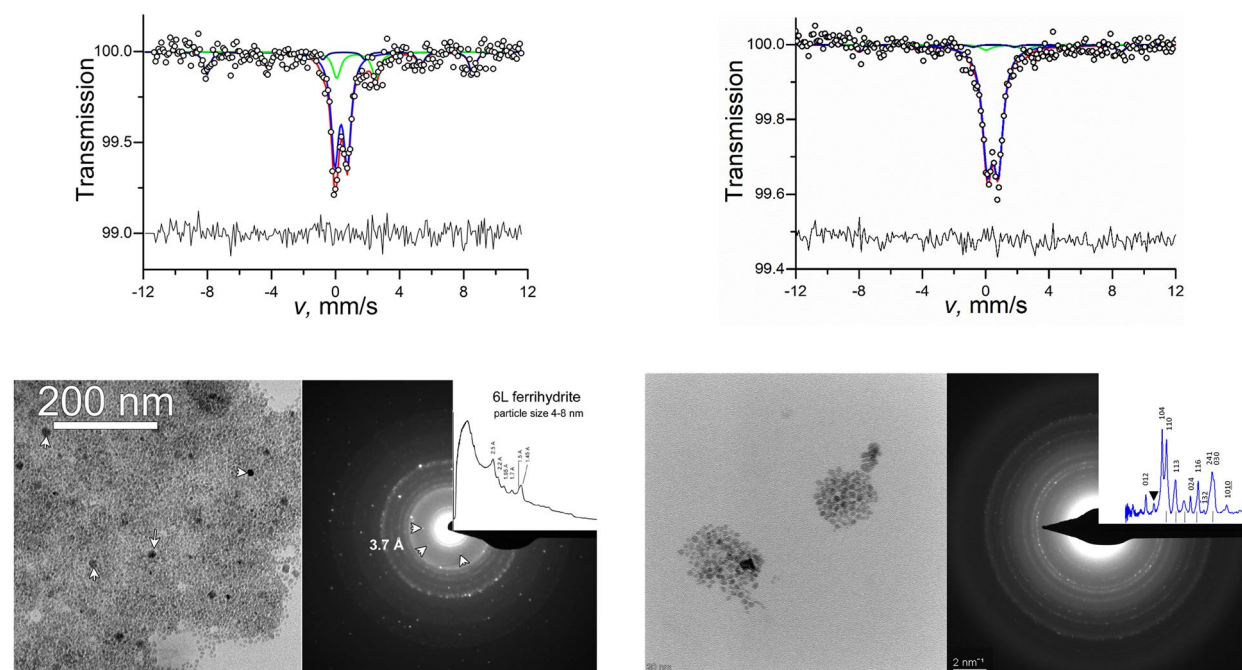

Figure 7: Mössbauer spectra, bright-field images, and SAED patterns of suspension S3 shortly after preparation (left) and 6 years after (right). White arrows indicate faint diagnostic reflections for minor component hematite. Diffraction peak at ca. 3 Å (black arrowhead) can be identified as maghemite.
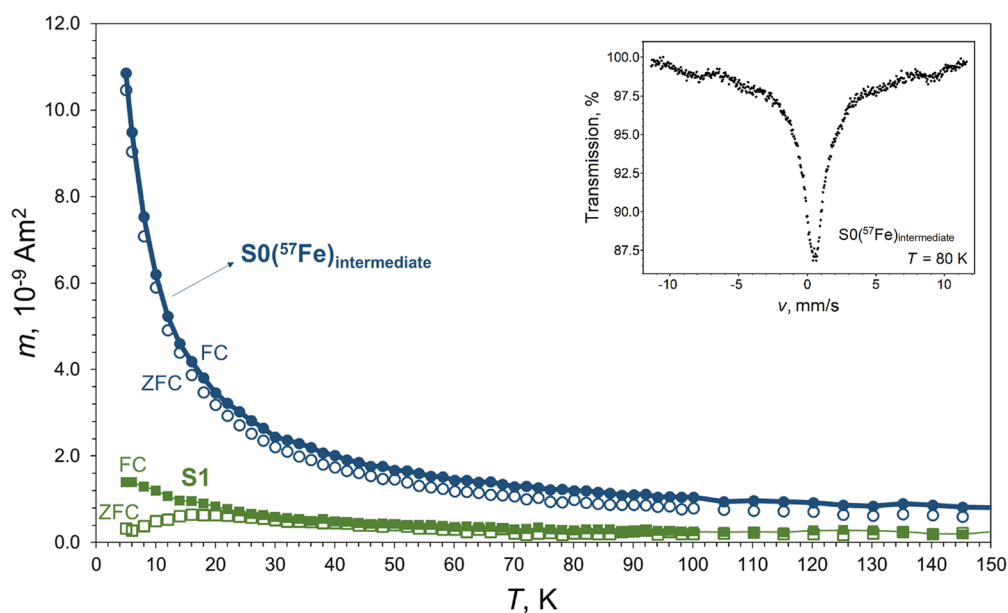
Figure 8: Comparison of FC/ZFC magnetization curves of the samples S1 and S0(^{57}Fe)$_{intermediate}$, measured ca. 20 months after the first TEM and ^{57}Fe Mössbauer measurements were carried out on sample S1 (Fig. 5 left). Analogous measurements on the samples S2 and S3 resulted in magnetization curves (Suppl. Fig. 1) lying close to those of S1, and are therefore omitted here for clarity. The inset shows the ^{57}Fe Mössbauer spectrum of S0(^{57}Fe)$_{intermediate}$ measured at 80 K.

in antiferromagnetic or weakly ferromagnetic hematite or in speromagnetic ferrihydrite nanoparticles in these nanocolloid suspensions. By comparing the obtained FC/ZFC magnetization curves with those of dried 2-lines and 6-lines ferrihydrite nanoparticle powders [12], in the latter case we find similar magnetic blocking and irreversibility behavior, though the respective temperatures are higher than in our case (e.g., T_b = 49 K and 46 K for 2-lines and 6-lines ferrihydrite, respectively [12]). The lower blocking and irreversibility temperatures in our case could be due to the fact that our samples were applied in the form of a solution to the blotting paper that could be let dry without promoting close contact among the individual nanoparticles, in contrast with cases where a precipitate is dried in the form of a powder of interacting nanoparticles. Magnetic interparticle interactions are therefore expected to play a smaller role in influencing the magnetic response of our samples. The latter is indeed confirmed by the increasing tendency of FC magnetization with decreasing temperature even at temperatures below T_b. At the same time, the obtained magnetization curves are similar to those obtained for weakly- or non-interacting hematite nanoparticles [25, 26], even by considering the blocking temperature. By taking into account also the similarity of FC/ZFC curves obtained for the S1, S2, and S3 samples (Suppl. Fig. 1), this may indicate that the nanoparticles applied to the blotting paper transformed to hematite during the course of drying. Nevertheless, comparison of the ZFC curves of S1, S2, and S3 with that of S0(^{57}Fe)$_{intermediate}$ (Fig. 8) makes it obvious that the transformation of nanoparticles undergoing in the suspensions

according to Figs. 5, 6, and 7 proceeds without the formation of appreciable amounts of paramagnetic iron species. Iron in the studied nanoparticles can therefore be regarded as having negligible solubility in their respective suspensions.

Biological utilization of the nanoparticles in the plant model

The utilization of the different nanomaterial compounds was tested by the suppression of Fe deficiency responses in the plant model. Results indicate that under biological conditions the suspensions are suitable to be used as an effective source of Fe in restoring plant Fe deficiency. The responses were studied in a more detailed manner for suspension S0 right after preparation (containing only nanoparticles of ferrihydrite and referred to as NFH) and S0 at a late stage of transformation (containing only nanoparticles of hematite and referred to as NH). The expression of *CsFRO1* was chosen as indicator of Fe deficiency responses, as it is the most sensitive root ferric chelate reductase for Fe resupply. Total activity of root ferric chelate reductases was measured as root FCR activity. In the expression of *CsFRO1* [Fig. 9(a)], both the treatment with NFH and NH induced a sharp decrease. In 24 h of treatment, the relative transcript amount decreased significantly comparing to the untreated Fe-deficient plants, but the difference between NFH- and NH-induced changes remained not significant. In the FCR activity in 24 h no differences were detected among Fe-deficient plants and treated plants (not shown). However, 48 h of treatment induced
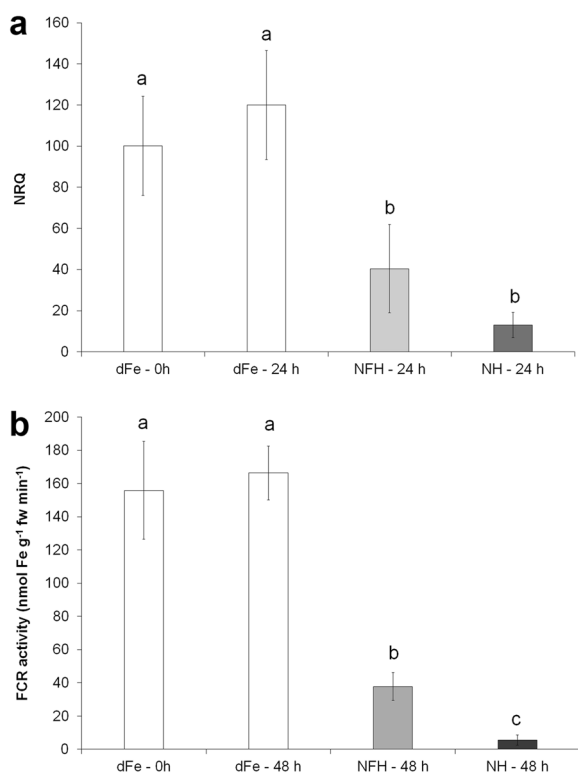
Figure 9: Normalized relative quantity (NRQ) of *CsFRO1* transcript amount (a) and ferric chelate reductase (FCR) activity (b) in the roots of Fe-deficient (dFe), nanoferrihydrite (NFH)-treated, and nanohematite (NH)-treated plants. Error bars represent SD values. To compare the differences, one-way ANOVA was performed with Tukey–Kramer *post hoc* tests on the treatments ($P < 0.01$). Statistical groups are indicated with letters.

a considerable decrease in the root FCR activity too, in comparison to untreated Fe-deficient plants [Fig. 9(b)]. In contrast to expression data, a remarkable difference was found in the FCR activity among NFH- and NH-treated plants where the NH treatment resulted in a stronger suppression of the activity.

Discussion

While the formation of hematite proceeds via aggregation and dehydration of ferrihydrite nanoparticles, that of goethite requires dissolution of ferrihydrite and subsequent nucleation and crystallization processes utilizing the iron(III) ions dissolved in the solution. With decreasing pH levels, a gradual inhibition of the latter process sets in below pH ≈ 4, and consequently the formation of hematite becomes increasingly favored upon further reduction of pH [13]. At the pH level of our sample, the formation of goethite is expected to outweigh that of hematite. However, the result observed suggests the opposite. In the case of S0, S1, S2, and S3 prepared using the same protocol but different surfactants the result of the transformation was found to be only hematite. Magnetic measurements also confirmed that

no dissolution preceding goethite formation takes place in these samples. On the other hand, in S0(^{57}Fe) which was prepared with the same surfactant as S0, the final material was a mixture of hematite and goethite with the prevalence of goethite. The ratio of hematite to goethite in S0(^{57}Fe) is in close agreement with the values reported in [14] for suspensions of pH 2.5 after 441 day after preparation. Not only the ratio of minerals varied in different suspensions but also the size of the formed hematite particles was found to be different at the final stage of transformation, while in the case of S2 the particles are over 20 nm, in samples S0, S1, and S3, the particles are much smaller (mostly less than 10 nm). Moreover, among the samples only S3 displayed the presence of a minor amount of maghemite.

The appearance of a minor iron(II) component may be due to the reducing effect of the surfactant, applied in relatively low concentration, given that polyethylene glycols may act as a reducing agent [27]. A reductant may induce interfacial electron transfer to structural iron(III) and accelerate the transformation of ferrihydrite to a mixed-valence compound [28, 29], which dissolves more readily and facilitates the formation of goethite and feroxyhyte (δ-FeOOH), an apparently rare iron(III) oxide with a local structure that has been described as a highly disordered variant of hematite [15]. Based on the obtained Mössbauer parameters and applied protocol of preparation the formed mixed-valence compound may be identified as chlorinated green rust [30, 31]. Earlier this mineral was suggested to form during the transformation of ferrihydrite as an intermediate product [13].

The results obtained allow one to estimate the conversion half-life of ferrihydrite for different nanocolloid materials. The time dependence of percentage of ferrihydrite remained was fitted by suggesting first-order rate kinetics. Calculated time of half transformation for S0(^{57}Fe) is 480 ± 40 days. Good agreement between the experimental data and fit indicates that in this case, the transformation of ferrihydrite can be described by a first-order rate kinetics. It is remarkable that for S0, Mössbauer and TEM results are consistent with a ca. 1 year of half conversion time of ferrihydrite, which is comparable with the time calculated for S0(^{57}Fe). Previous studies [14] showed that the time for half conversion of ferrihydrite increases with decreasing pH levels and for a ferrihydrite suspension prepared at pH ≈ 2 without surfactant also reaches nearly 1 year. Samples, S1 and S3 prepared using the same protocol as S0 but other surfactants, exhibited slower transformation, while sample S2 showed the presence of significant amount of hematite already shortly after preparation. It is worth to point out explicitly that despite both S0 and S1 were prepared by adding polyethylene glycol polymer with a mean molecular mass of 200 and 1500 g/mol, respectively, the transformation rate varies significantly: S0 was almost fully transformed to hematite after 5 years, while S1 shows only a minor transformation in the same time interval.

This observation suggests that the type and, remarkably, the molar weight of surfactant play much more important roles for the transformation rate than the initial state of iron.

Based on these results one can estimate the ferrihydrite concentration of a suspension at any point of time with sufficient accuracy. This moderate rate of transformation presents an opportunity to perform biological experiments with nanocolloid suspensions having different ferrihydrite/goethite/hematite compositions by applying the same suspension at different points of time after its preparation as was done using suspension S0. Since the application of nanohematite (S0 after transformation) resulted in a stronger decline in these responses than nanoferrihydrite (S0 as-prepared), the data obtained suggest a slightly better availability of Fe from the suspension in the form of nanohematite. This observation may be connected not only to the changes in the structure and crystallinity of the particles but also to the change in the degree of coating of the particles with surfactants that is proposed to affect the interaction of nanocolloid particles and plasma membrane enzymes/secreted compounds responsible for the FCR action of plant roots. After transformation to hematite, which occurs via aggregation, the particles formed are not fully covered by the surfactant, which may lead to a more efficient Fe utilization by the roots. SAED patterns and bright-field images of the samples showed the presence of the residue of surfactants mostly not coating but just connecting particles with each other.

Conclusions

Comparison of several nanoscale ferrihydrite suspensions allowed to reveal the dependence of their transformation time and their final mineral composition on the type of the applied surfactant. The results obtained allow us to conclude the following:

- The type of the applied surfactant can influence the transformation attributes. Polyethylene glycol polymer with a mean molecular mass of 1500 g/mol was shown to be the best from the applied surfactants to preserve the initial structure and size of the particles;
- The transformation preserves the stability of the colloid suspensions (i.e., no precipitates) over several year-long time periods;
- Iron(II)-containing intermediate compounds were found to form in the case of all applied surfactants and may play a role in the transformation process;
- The end product hematite appears to be more effective in restoring plant Fe deficiency than ferrihydrite, thus, the aging of the nanocolloid system significantly affects the utilization of the Fe. This points out that beside the particle size and structure also the covering of these Fe nanoparticles

with surfactants plays an important role in their biological applicability, which should be taken into account in planning any long-term field applications.

Methods and materials

Preparation

The colloid suspension sample S0 was prepared via forced hydrolysis process [32] as follows. A solution of 0.5 M $FeCl_3 \times 6H_2O$ was prepared with a volume of 50 ml, along with a separate 30 ml solution of surfactant Priowax 200 (polyethylene glycol polymer with a mean molecular mass of 200 g/mol, Lamberti Chemicals, Gallarate, Italy). The latter solution was added to 600 ml deionized water at 80 °C, with subsequent 10-min stirring. The $FeCl_3$ solution was then added to the obtained surfactant solution at a rate of 2 ml/min, with an additional 2-h stirring at 80 °C.

In order to compare the effect of different surfactants three samples S1, S2, S3 were prepared using the same protocol but various surfactant solutions:

- S1 was prepared using PEG-1500 (polyethylene glycol polymer with a mean molecular mass of 1500 g/mol, Lamberti Chemicals, Gallarate, Italy);
- S2 was prepared using Emulsion 104D (polyoxyethylene–polyoxypropylene copolymer, Lamberti Chemicals, Gallarate, Italy);
- S3 was prepared using SOLUTOL HS 15 (polyoxyethylene ester of 12-hydroxystearic acid, BASF Pharma).

To achieve better statistics of Mössbauer spectra, the $S0(^{57}Fe)$ colloid suspension sample was prepared by using an $FeCl_3$ solution prepared from iron enriched in ^{57}Fe and surfactant Priowax 200. The first step of preparation was identical to that given above for S0. Following characterization of the resulted sample (denoted further on with $S0(^{57}Fe)_{intermediate}$) by TEM, magnetization measurement, and ^{57}Fe Mössbauer spectroscopy, a recrystallization step was performed in order to complete the formation of nanoparticles from the $^{57}FeCl_3$ solution. In this second step, the solution, at room temperature, was first diluted with distilled water to twice of its volume. The pH of the solution was then set to 7 with ammonia solution leading to the formation of precipitates. The pH of the solution was then adjusted to 1.75 with the addition of 10% (V/V) HCl solution, leading to partial dissolution of the precipitates. The resultant suspension was then boiled for 15 min, which led to the dissolution of all the precipitates and thereby to the formation of the colloid suspension used subsequently in the experiments.

The iron concentration of the colloid suspensions was measured by inductively coupled plasma optical emission

spectrometry. Iron concentrations and pH values measured after preparation are shown in Suppl. Table 1. During the investigation, the suspensions were stored in darkness in order to prevent any possible photoinduced transformation [33, 34].

Mössbauer spectroscopy

To reveal the composition of nanoparticles and the state of iron in the associated iron microenvironments in these nanocolloidal systems, ^{57}Fe Mössbauer spectroscopy measurements were performed on the frozen nanocolloid suspensions at $T = 80$ K using conventional Mössbauer spectrometers (WissEl, Starnberg, Germany and KFKI, Budapest, Hungary) operating in the constant acceleration mode. ^{57}Co source in Rh matrix, kept at ambient temperature, provided the γ-rays for the measurements. The samples were kept at low temperature either by using a bath-type cryostat (SVT-400-MOSS, Janis, Woburn, MA, USA) filled with liquid nitrogen, or by using a custom-made flow-through type, liquid nitrogen-cooled cryostat.

The Mössbauer spectra were evaluated by standard computer-based statistical analysis methods that included fitting the experimental data by a sum of Lorentzians using a least-squares minimization procedure with the help of the MossWinn 4.0i program [35]. The isomer shifts are given relative to that of α-Fe at room temperature.

Transmission electron microscopy

Transmission electron microscopy (TEM) and selected area electron diffraction (SAED) measurements of the as-prepared suspension samples were performed using a Philips CM20 TEM (LaB$_6$ cathode) operating at 200 keV [Figs. 5(a), 6(a), and 7(a)] and a JEOL 3010 UHR TEM equipped with a Gatan GIF Tridiem (LaB6 filament, 0.17-nm point resolution) operating at 300 keV [Fig. 2(a–c)]. TEM study of the aged samples was done by the means of a FEI-Themis 200 G3 transmission electron microscope with a C$_s$ corrected objective lens (FEG electron source, point resolution 0.07 nm in HRTEM mode) operating at 200 keV. Suspension samples for the TEM analysis were prepared using ethanol. A drop of the resulting suspension was deposited onto ultrathin carbon-coated copper TEM grid (Ted Pella). The HRTEM images were analyzed using Velox (FEI) software.

SAED patterns were taken using 200-μm-sized aperture, resulting in diffraction area of ca. 3 μm diameter. This setup ensures that enough large number of nanocrystals are included into the diffraction measurements, which is necessary for good statistics.

Integrated intensity profiles were obtained using Process Diffraction software [36]. Background subtraction was performed using Origin software. For hematite and ferrihydrite,

crystallographic data of Blake et al. [37] and Jansen et al. [23] were used, respectively.

Magnetic measurements

FC/ZFC magnetization measurements of samples S1, S2, S3, and S0(^{57}Fe)$_{intermediate}$ were carried out in the temperature range of 5…300 K by using a MPMS-5S Quantum Design superconducting interference device. In each case 100 μL suspension was dropped on a piece of blotting paper having the same size and shape (an oblong rectangle) for all the samples. After the blotting papers dried, they were coiled up to form cylindrical columns of ca. 1 cm height, and were then subsequently measured in this form. In order to be able to separate the magnetic response of the magnetic species in the suspensions from that of the blotting paper, a blotting paper column was also prepared and measured without the addition of any suspension. The samples were cooled from 300 to 5 K either in zero external magnetic field (ZFC) or in the measuring field of $H = 10$ Oe (FC). The magnetization was then measured as a function of temperature by applying the $H = 10$ Oe measuring field upon heating. In the final results, the magnetization level of the suspension-free blotting paper column was subtracted from the magnetization levels obtained for the samples under investigation.

Plant material

Strategy I model cucumber (*Cucumis sativus* L. cv. Joker F1) was applied. Germination was performed in darkness at 26 °C for 2 days. Seedlings were transferred to 0.5 mM CaSO$_4$ for 24 h in darkness. Cultivation of plant material was performed on ¼ Hoagland solution (1.25 mM KNO$_3$; 1.25 mM Ca(NO$_3$)$_2$; 0.5 mM MgSO$_4$; 0.25 mM KH$_2$PO$_4$; 11.6 μM H$_3$BO$_3$; 4.5 μM MnCl$_2$; 0.19 μM ZnSO$_4$; 0.12 μM Na$_2$MoO$_4$; 0.08 μM CuSO$_4$) where the medium was free of any Fe sources. Nutrient solution in the 400 ml pots was replaced 3 times per week. Environmental parameters in the growth chamber were 14-h light (120 μmol m^{-2} s^{-1} photosynthetic photon flux density)/10-h darkness, relative humidity of 75/70%, temperature of 24/22 °C. Light periods started at 6 am. Nanomaterial colloidal suspensions were applied in 20 μM nominal concentration of iron on 3-week-old plants. Recovery treatments started exactly at 9:00 am in each repetition.

Ferric chelate reductase assay

Ferric chelate reductase (FCR) assay was applied as in Kovács et al. [17]. The absorbance of the [Fe(II)-bathophenanthroline disulfonate$_3$]$^{4-}$ complexes (extinction coefficient of 22.14 mM^{-1} cm^{-1}; [38]) was measured at 535 nm (UV-2100, Shimadzu, Kyoto, Japan).

Quantitative RT-PCR

Polyadenylated RNA (considered as mRNA) fraction was isolated using the GenoVision mRNA isolation kit (Qiagen) according to the manufacturer's instructions from root samples. After recovery, mRNA samples were separated in 25 µl diethyl pyrocarbonate-treated deionized water. RNA content was measured by NanoDrop1000 (Thermo-Fisher Scientific). To eliminate residual genomic DNA contamination, RNase-free DNase I (Thermo-Fisher Scientific) digestion was applied. Reverse transcription was performed by RevertAid Reverse Transcriptase (Thermo-Fisher Scientific) with oligo-dT primers at 42 °C for 45 min and 70 °C for 10 min. *CsACT*, *CsEF1A* and *CsFRO1* sequences were accessed in *C. sativus* database [39] and in CuGenDB [40]. Primer sequences, listed in Suppl. Table 4, were designed using NCBI tool. Quantitative RT-PCR were performed in StepOnePlus Real-Time PCR system (Applied Biosystems) operating with StepOne™ v.2.2.3 software as in Müller et al. [41]. Analysis was performed according to Pfaffl [42].

Statistical analysis

Measurements were repeated in 3 independent biological repetitions where all samples were mixed of 6 plant individuals of identical phenological stage. For qRT-PCR, 4 parallel RNA technical replicates were isolated in 3 independent experiments (biological replicates). One-way ANOVA tests with Tukey–Kramer *post hoc* tests were performed on data using InStat v. 3.00 (GraphPad Software, Inc., San Diego, CA, USA). The term 'significantly different' means that the similarity of samples is $P < 0.01$.

Funding

Data availability

The datasets generated during and/or analyzed during the current study are available from the corresponding author on reasonable request.

Declarations

Conflict of interest On behalf of all authors, the corresponding author states that there is no conflict of interest.

Open Access

Supplementary Information

The online version contains supplementary material available at https://doi.org/10.1557/s43578-022-00686-z.

References

1. D.G. Merkel et al., Nanoscale (2015). https://doi.org/10.1039/C5NR02928G
2. D.G. Merkel et al., Mater. Res. Express (2019). https://doi.org/10.1088/2053-1591/ab1c84
3. J. Kalt et al., Phys. Rev. B (2020). https://doi.org/10.1103/PhysRevB.102.195414
4. D.G. Merkel et al., Sci. Rep. (2020). https://doi.org/10.1038/s41598-020-70899-x
5. K.T. Nguyen et al., J. Mat. Res. (2021). https://doi.org/10.1557/s43578-020-00011-6
6. J.A. Hernandez-Viezcas et al., ACS Nano (2013). https://doi.org/10.1021/nn305196q
7. A. Bour et al., J. Hazard. Mat. (2015). https://doi.org/10.1016/j.jhazmat.2014.10.021
8. A. Ebrahiminezhad et al., Green Process. Synth. (2017). https://doi.org/10.1515/gps-2016-0133
9. H. Tombuloglu et al., Chemosphere (2019). https://doi.org/10.1016/j.chemosphere.2019.03.075
10. H. Tombuloglu et al., Environ. Nanotechnol. Monit. Manag. (2019). https://doi.org/10.1016/j.enmm.2019.100223
11. P. Sipos et al., J. Soils Sediments (2021). https://doi.org/10.1007/s11368-021-02899-x
12. D. Carta et al., Mater. Chem. Phys. (2009). https://doi.org/10.1016/j.matchemphys.2008.07.122
13. R.M. Cornell, U. Schwertmann, *The Iron Oxides: Structure, Properties, Reactions, Occurrences, and Uses*, vol. 2 (Wiley, Weinheim, 2003)
14. U. Schwertmann, E. Murad, Clays Clay Miner. (1983). https://doi.org/10.1346/CCMN.1983.0310405
15. K. Hockmann et al., Environ. Sci. Technol. (2021). https://doi.org/10.1021/acs.est.0c08660

16. J. Yan, A.J. Frierdich, J.G. Catalano, Geochim. Cosmochim. Acta (2022). https://doi.org/10.1016/j.gca.2022.01.014

17. K. Kovács et al., Planta (2009). https://doi.org/10.1007/s00425-008-0826-x

18. L. Marastoni et al., Plant Physiol. Biochem. (2019). https://doi.org/10.1016/j.plaphy.2019.01.013

19. J. Rodríguez-Celma et al., Front. Plant Sci. (2019). https://doi.org/10.3389/fpls.2019.00098

20. J. Spielmann, G. Vert, J. Exp. Bot. (2021). https://doi.org/10.1093/jxb/eraa441

21. A. Singh et al. to be published

22. Z. Homonnay et al., Hyperfine Interact. (2016). https://doi.org/10.1007/s10751-016-1334-1

23. E. Jansen et al., Appl. Phys. A (2002). https://doi.org/10.1007/s003390101175

24. J.G. Stevens, *Mössbauer mineral handbook* (Mössbauer Effect Data Center, Asheville, 1998)

25. M. Tadic et al., J. Alloys Compd. (2007). https://doi.org/10.1016/j.jallcom.2006.09.099

26. D. Zysler, M. Vasquez Mansilla, D. Fiorani, *Eur* (J. B, Phys, 2004). https://doi.org/10.1140/epjb/e2004-00306-7

27. C. Luo et al., J. Colloid Interface Sci. (2005). https://doi.org/10.1016/j.jcis.2005.03.005

28. R.M. Cornell, W. Schneider, R. Giovanoli, Polyhedron (1989). https://doi.org/10.1016/S0277-5387(00)80544-6

29. J.P.H. Perez et al., Environ. Sci. Nano (2021). https://doi.org/10.1039/D1EN00384D

30. Ph. Refait et al., Hyperfine Interact. (1992). https://doi.org/10.1007/BF02401957

31. N. Van Groeningen et al., Environ. Sci.: Process. Impacts (2020). https://doi.org/10.1039/D0EM00063A

32. E. Matijevic, Annu Rev. Mater. Sci. (1985). https://doi.org/10.1146/annurev.ms.15.080185.002411

33. M. Gracheva et al., Photochem. Photobiol. Sci. (2022). https://doi.org/10.1007/s43630-022-00188-1

34. S.O. Pehkonen, R.L. Siefert, M.R. Hoffmann, Environ. Sci. Technol. (1995). https://doi.org/10.1021/es00005a012

35. Z. Klencsár, E. Kuzmann, A. Vértes, J. Radioanal. Nucl. Chem. (1996). https://doi.org/10.1007/bf02055410

36. J.L. Lábár, Microsc. Microanal. (2008). https://doi.org/10.1017/S1431927608080380

37. R.L. Blake et al., Am. Miner. **51**, 123–129 (1966)

38. G.F. Smith et al., Analyst (1952). https://doi.org/10.1039/AN9527700418

39. https://phytozome.jgi.doe.gov/pz/portal.html

40. http://cucurbitgenomics.org

41. B. Müller et al., Planta (2019). https://doi.org/10.1007/s00425-018-3037-0

42. M.W. Pfaffl, Nucleic Acids Res. (2001). https://doi.org/10.1093/nar/29.9.e45

13